# THERMO-MECHANICAL MODEL OF THE FRICTION STIR WELDING PROCESS AND ITS APPLICATION FOR THE ALUMINIUM ALLOY AA5754

U. REISGEN*, A. SCHIEBAHN*, A. NAUMOV*,
A. MASLENNIKOV* and V. EROFEEV**

** RWTH Aachen University, ISF-Welding and Joining Institute, 52062 Aachen, Germany, schiebahn@isf.rwth-aachen.de*
*** Tula State University, Welding department, 300012 Tula, Russian Federation, va_erofeev@mail.ru*

*DOI 10.3217/978-3-85125-615-4-30*

ABSTRACT

A thermo-mechanical model of the FSW process for the investigation of the visco-plastic flows produced in the stir zone has been developed. It takes into account the frictional and volumetric heat sources. The input characteristics of the dynamic viscosity and shear stress for AA5754 were determined during specially designed FSW-alike experiments. The obtained distributions of the temperature, relative pressure, strain rate, viscous flow velocities, as well as the values of the longitudinal and transversal tool force components agree qualitatively with the literature data.

Keywords: friction stir welding (FSW), aluminium alloy AA5754, plastic deformation, finite difference method, experimental procedure, comparison

## INTRODUCTION

The FSW process is a variant of pressure welding and entails considerable plastic deformation. The process temperatures do not exceed 80% of the workpiece liquidus temperature [1, 2]. In friction stir welding a non-consumable rotating tool with a specially designed pin and shoulder is inserted into the abutting edges of workpieces to be joined and traversed along the line of the joint [3]. As the tool travels, heat is created by the contact friction between the shoulder, pin and the workpiece as well as by the plastic deformation of the material in the workpiece zone around the pin, where the material dwells in a visco-plastic condition – the stir zone (SZ). The plasticized material is stirred around the pin, forming behind a continuous weld seam.

The FSW process represents a combination of two tightly connected physical phenomena of mechanical and thermal treatment (friction, heat generation, and considerable visco-plastic metal flow), fig. 1.

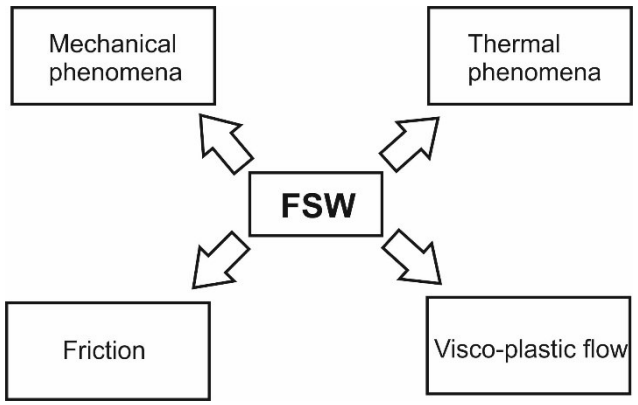


**Fig. 1** A scheme of interaction of mechanical and thermal phenomena in FSW.

The produced visco-plastic metal flows in the SZ influence, among others, the volumetric heat generation, thermal cycles in the workpiece metal, microstructure, mechanical properties and the final shape of the weld. These technological aspects are very important for producing sound welded joints [4]. Therefore, for a better understanding of the FSW process, one has to provide an analysis of the thermal and mechanical physical phenomena and their combined action on the primary internal characteristics of the FSW process i.e. heat generation, temperature distribution and viscous flow velocities in the SZ. It is planned to perform the investigation, among others, with the help of numerical modelling of the thermal and mechanical physical phenomena in the SZ on the basis of a thermo-mechanical model of the FSW process. For this purpose the model must be self-consistent and flexible to enhancement. It must consider the influence of main process parameters on the thermo-mechanical condition of the material in the SZ by means of computing the thermal, velocity and pressure fields.

The first studies were based on heat conduction, ignoring the plastic flow near the tool [5, 6]. Schmidt et al. [7] proposed a general analytical model for the heat generation during the FSW of 2024-T3 aluminium alloy. Friggard at al. [8] assumed that frictional heating at the tool shoulder-workpiece interface was entirely responsible for the heat generation during welding. Chao et al. [9] estimated the fraction of the heat generated at the tool-shoulder interface, being transported into the workpiece during the FSW of an aluminium alloy, considering the overall heat balance in the tool as well as in the workpiece with the usage of inverse modelling.

Seidel and Reynolds [10] developed a 2D fully coupled steady-state thermal model based on laminar, viscous and non-Newtonian flow around a circular cylinder. Moreover, they considered only one heat source in the form of viscous dissipation in the stirring zone, omitting the heat generation between the tool shoulder and the workpiece surface. Colegrove and Shercliff [11, 12] used a commercial software FLUENT to develop a 3D thermal and material flow model for the FSW of the AA7075 alloy. They used temperature-independent physical-mechanical properties of the alloy. Tutunchilar et al. [13] developed a valuable 3D Lagrangian finite element model by using the software DEFORM 3D for predicting the material flow in the FSW. The authors were able to show the material flow patterns in the center, advancing and retreating sides of the tool. The authors [14] provided

a 2D FSW model, based on the smoothed particle hydrodynamics (SPH) with an assumption that effective viscosity depends only on temperature. Later this model was improved by adding the Sellars-Tegart constitutive material law [15]. Despite the fact that large plastic deformation, defect formation and material mixing can be well captured by this method, the main its disadvantage is that to achieve the same accuracy as in the grid-based methods, the number of discretization points in SPH should be larger, the computational time and costs therefore increase [15].

One of the basic finite difference models of the FSW process was developed in the works [16, 17]. In the present paper, we have explicitly taken into consideration the frictional heat source in the contact between the tool shoulder and the workpiece surface. We present the visco-plastic flow of the metal around the pin in the stir zone as an incompressible viscous fluid flow. Internal friction between the layers of the plasticized metal causes the volumetric heat generation. At high strain rates, typical for the FSW conditions, the metals undergo work hardening, the rate of which is equivalent to the dynamic viscosity. This circumstance allows us to consider the metal, dwelling at pressures exceeding its yield stress, as a viscous fluid. The values of the dynamic viscosity and shear stress were obtained from a series of FSW-alike experiments. Hence, metal in the stir zone is treated as a highly viscous non-Newtonian fluid, with its dynamic viscosity dependent on both the temperature and the strain rate.

## PROBLEM STATEMENT

The objective of the present work was a numerical investigation of the thermal and mechanical physical phenomena, accompanying FSW, as well as their combined influence on the primary internal characteristics of the FSW process i.e. heat generation, temperature distribution and visco-plastic flow velocities in the SZ. The object for the investigation was a typical FSW system, consisting of a workpiece (butt joint 1.5+1.5 mm made of the aluminium alloy AA5754), anvil (AA6082, thickness 20.0 mm), and a working tool with a threadless pin in a form of a truncated cone, fig. 2.

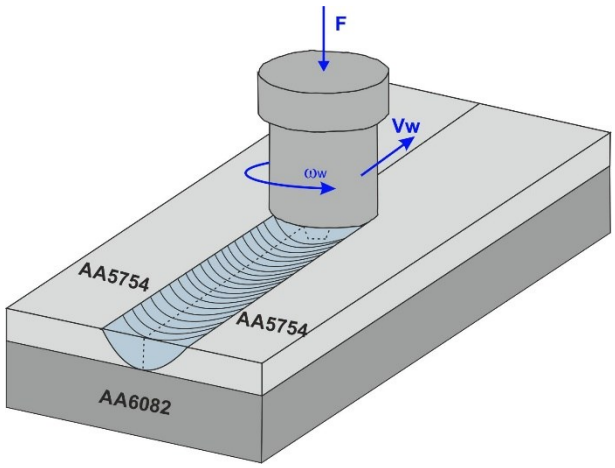

**Fig. 2** The FSW scene, being used for the modelling (schematic).

## COORDINATE SYSTEM, MODELLING SPACE

As the FSW process involves a circular motion of both the tool and visco-plastic flow around the tool pin, we have chosen a cylindrical coordinate system in the Eulerian formulation with the vertical axis coinciding with the tool rotation axis, fig. 3.

The modelling space comprises a few modelling zones differing with their physical properties: $W_1$, $W_2$ is the workpiece metal (further, during the text a unified designation for both sheets is used – $W$, as the metal of both sheets is the same); $P$ is the workpiece metal in the plastic condition (stir zone); $P_w$ is the weld seam metal; $T_p$ is the tool metal; $B$ is the anvil; $A$ is the air.

The coordinates of these zones are beforehand unknown and determined with accordance to the tool geometry and the interface boundaries $W \cap T_p$, $W \cap B$, $W \cap A$, $T_p \cap A$ (where the symbol $\cap$ means the intersection of the corresponding zones). The location of the SZ relative to the workpiece metal $W - W \cap P$ is also unknown in advance and defined during the solution of the model equations.

The dimensions of the modelling finite difference mesh are determined in dependence on the sizes of the workpiece. In the $Z$-direction (mesh index $k$) it was accepted that $dz=S/15$ ($S$ is the workpiece thickness). In the angular direction (mesh index $j$) the step $d\varphi=2\pi/60=\pi/30$. In the radial direction (mesh index $i$), the step was taken variable and increasing with moving away from the pin surface as: $r_i=1.1r_{i-1}$. The dimensions of the computational mesh ($i_{max}\times j_{max}\times k_{max}$) are $36\times60\times15$.

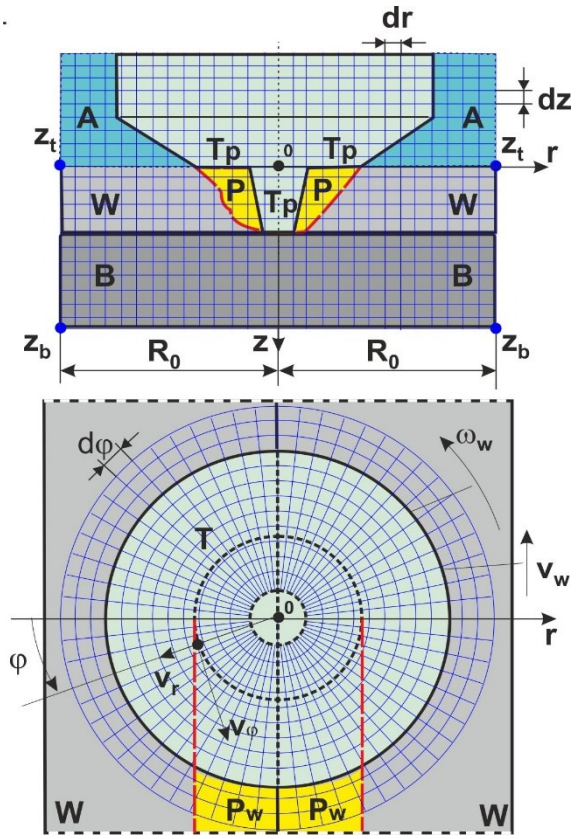


**Fig. 3** Schematic representation of the structure of the modelling space.

## BASIC MODEL EQUATIONS

### ENERGY CONSERVATION EQUATION

During the FSW process, the two main sources generate the heat energy: the first source is the contact friction between the surfaces of the tool shoulder and workpiece, the second one is the plastic deformation process in the bulk of the SZ [18]. The produced heat energy redistributes with the help of heat conduction and flow of the visco-plastic metal around the pin. These phenomena are described by the energy conservation equation in the following non-stationary formulation

$$\frac{\partial H}{\partial t} + div\left(\rho \vec{v} H\right) = div\left(\lambda grad T\right) + q_{\Sigma} \tag{1}$$

where $H$ is the temperature-dependent specific enthalpy; $\rho$ is the density; $\vec{v}$ is the velocity vector of the substance; $\lambda$ is the temperature-dependent thermal conductivity; $T$ is the temperature; $q_\Sigma$ is the total heat generation rate.

The boundary conditions for Eq. 1 applied are as follows (see fig. 3)

$$\begin{aligned}
&\frac{\partial T}{\partial r} = 0,\ r = R_0,\\
&-\lambda\frac{\partial T}{\partial z} = q_{sh},\ z = z_t, r \in [r_s \ldots r_{ss}],\ q_{sh} = \pi\omega_w\sigma_{cont}\frac{2}{3}\left(r_{ss}^3 - r_s^3\right)dz,\\
&\lambda\frac{\partial T}{\partial z} = \tilde{\ } \qquad\qquad T_0^4\right) + \alpha_t\left(T - T_0\right),\ z = z_t, r \in [r_{ss} \ldots R_0],\\
&\frac{\partial T}{\partial z} = 0,\ z = z_b,
\end{aligned} \tag{2}$$

where $\tilde{\ }$ is the emissivity factor; $q_{sh}$ is the heat input from the tool shoulder surface; $\sigma_0$ is the Stefan-Boltzmann constant; $T_0$ is the environment temperature; $\alpha_t$ is the convective heat transfer coefficient.

The temperature-dependent thermo-physical properties of the metal at the different modelling zones depend on the location of the considered point to one of the modelling zones (see fig. 3) as follows

$$\lambda = \begin{cases} \lambda_w(T) & for \quad r,\varphi,z \in W,P_w \\ \lambda_p(T) & for \quad r,\varphi,z \in P,P_w \\ \lambda_B(T) & for \quad r,\varphi,z \in B \end{cases}$$
$$H = \begin{cases} H_w(T) & for \quad r,\varphi,z \in W,P_w \\ H_p(T) & for \quad r,\varphi,z \in P,P_w \\ H_B(T) & for \quad r,\varphi,z \in B \end{cases} \tag{3}$$

Internal friction in the SZ initiates a volumetric heat source [19]

$$q_{in} = \tau_T\left(T, \dot{\ }, \dot{\ }\right) \cdot \sqrt{2\left[\left(\frac{\partial v_r}{\partial r}\right)^2 + \left(\frac{1}{r}\frac{\partial v_\varphi}{\partial r} + \frac{v_r}{r}\right)^2 + \left(\frac{\partial v_z}{\partial z}\right)^2 + \right.}$$
$$\left. \sqrt{3\left[\frac{1}{2}\left(r\frac{\partial\left(v_\varphi/r\right)}{\partial r} + \frac{1}{r}\frac{\partial v_r}{\partial\varphi}\right)^2 + \frac{1}{2}\left(\frac{\partial v_z}{\partial r} + \frac{\partial v_r}{\partial z}\right)^2 + \frac{1}{2}\left(\frac{\partial v_\varphi}{\partial z} + \frac{1}{r}\frac{\partial v_z}{\partial\varphi}\right)^2\right.}\right) \tag{4}$$

where $\tau_T\left(T,\dot{}\right.$ is the temperature-and-strain-rate dependent shear yield strength; $\dot{}$ is effective the strain rate in the SZ; $\left(v_r(r,\varphi,z), v_\varphi(r,\varphi,z), v_z(r,\varphi,z)\right) \in P$are the components of the flow velocity vector $\vec{v}$.

The authors [20, 21] applied the concept of describing the tool geometry with cylindrical and taper pin configurations. Taking into account this concept, the heat source from the contact friction between the pin surface and workpiece is given as, fig. 4.

$$q_{cont} = \pi\omega_w\sigma_{cont}\left(\frac{1}{2}\left(r_s^2 + r_e^2\right)\frac{z_b}{\cos(\alpha)} + \frac{2}{3}r_e^3\right), \tag{5}$$

where the contact stress $\sigma_{cont}$ depends on the contact conditions at the interface tool surface-SZ and in general form can be written as [20]

$$\sigma_{cont} = \delta\tau_T\left(T,\dot{}\right. \quad F \quad S_{cont},$$

where $\sigma_{cont}$ is the contact stress; $\delta$ is the contact state variable (1 – sticking condition, 0 – slipping condition, in the model it was taken 0.65); $\mu$ is the coefficient of contact friction was set in modelling to 0.35-0.40; $\alpha$ is the pin angle; $F$ is the axial force; $S_{cont}$ is the contact area being determined as follows

$$S_{cont} = \begin{cases} \pi r^2, r \in [0...r_e] \\ r d\varphi dz \sin(\alpha),\ r \in [r_e...r_s] \end{cases}.$$

Hence, the total heat input in Eq. 1 is $q_\Sigma = q_{in} + q_{cont}$.

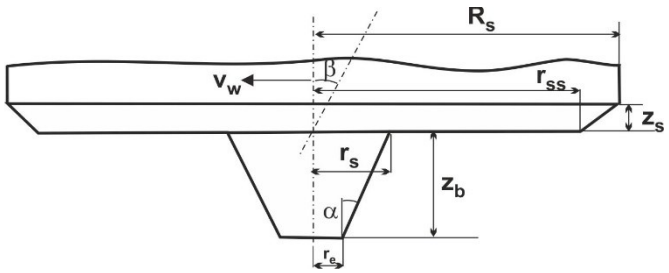


**Fig. 4** Schematic tool geometry being used for the modelling: $R_s$ = 11.0 mm, $r_{ss}$ = 4.0 mm, $r_s$ = 1.7 mm, $z_s$ = 12.0 mm, $z_b$ = 1.1 mm, $r_e$ = 1.5 mm, α = 10°, β=0°.

## NAVIER-STOKES EQUATION

The plastic flow velocities are determined from solving the Navier-Stokes equation written in the form

$$\frac{\partial v_r}{\partial t} + div\left(v_r \vec{v}\right) = -\left( -\frac{\partial p}{\partial r} + \eta\left( \frac{\partial^2 v_r}{\partial r^2} + \frac{\partial^2 v_r}{\left(r\partial\varphi\right)^2} + \frac{\partial^2 v_r}{\partial z^2} \right) \right), \tag{6}$$

$$\frac{\partial v_\varphi}{\partial t} + div\left(v_\varphi \vec{v}\right) = -\left( -\frac{\partial p}{r\partial\varphi} + \eta\left( \frac{\partial^2 v_\varphi}{\partial r^2} + \frac{\partial^2 v_\varphi}{\left(r\partial\varphi\right)^2} + \frac{\partial^2 v_\varphi}{\partial z^2} \right) \right), \tag{7}$$

$$\frac{\partial v_z}{\partial t} + div\left(v_z \vec{v}\right) = -\left( -\frac{\partial p}{\partial z} + \eta\left( \frac{\partial^2 v_z}{\partial r^2} + \frac{\partial^2 v_z}{\left(r\partial\varphi\right)^2} + \frac{\partial^2 v_z}{\partial z^2} \right) \right), \tag{8}$$

$$\frac{\partial v_\varphi}{r\partial\varphi} + \frac{1}{r}\frac{\partial (r v_r)}{\partial r} + \frac{\partial v_z}{\partial z} = 0, \tag{9}$$

where $p$ is the pressure in the SZ, determined with the help of the continuity equation (9); $\eta = \eta\left(T, \dot{\ }\right)$ is the temperature-and-strain-rate dependent dynamic viscosity.

At the boundary surface $P \cap W$ (see fig. 3), separating the stir zone from the rest of the workpiece metal, it was taken in the Eulerian reference frame

$$v_r = -v_w \sin\left(\varphi\right),\ v_\varphi = v_w \cos\left(\varphi\right),\ v_z = 0. \tag{10}$$

At the boundary surface $P \cap T_p$ separating the plastic strain zone and the pin metal, the flow velocity components are determined by the tool geometry (see fig. 3) and given as follows

$$\vec{v} = \begin{cases} \tilde{\ } \quad \text{n}\left(\varphi\right) & for\ \ r \in \left[r_e \ldots r_{ss}\right], \\ \tilde{\ } \quad \dfrac{r}{r_{ss}} \delta - v_w \cos\left(\varphi\right) & for\ \ r \in \left[r_e \ldots r_{ss}\right], \\ \tilde{\ } & for\ \ r \in \left[r_e \ldots r_{ss}\right], \end{cases} \tag{11}$$

where $\tilde{\ }$, $\tilde{\ }$, $\tilde{\ }$ are the radial, tangent and axial velocity components at the tool surface.

## DETERMINATION OF THE STIR ZONE BOUNDARY

We applied the von Mises criterion for determining the stir zone boundary. The coordinates of the SZ are calculated through the following variation procedure

$$3\tau_{P\cap W}^2 + \left(p + p_N\right)^2 \xrightarrow[P\cap W=\text{var}]{} \sigma_T^2, \tag{12}$$

where $\tau_{P\cap W}$ is the shear stress produced by the flow at the boundary; $p_N$ is the axial pressure from the tool; $p$ is the dynamic pressure being obtained from solving the equations (6-9); $\sigma_T$ is the yield strength.
The value of the shear stress at the boundary $P\cap W$ is calculated as

$$\tau_{P\cap W} = \eta \cdot grad\,\vec{v}. \tag{13}$$

The axial pressure $p_N$ is defined from solving the following integral equation

$$\iint_S \max\left(p_N, \tau_T\right) dS \xrightarrow[p_N=\text{var}]{} F, \tag{14}$$

describing the equilibrium condition between the axial force $F$ and the pressure $p_N$ within the contact working area $S$ between the tool and the workpiece.

## TOOL FORCES AND TORQUE

The longitudinal $F_l$ and transversal $F_t$ components of the total force acting on the tool depend on the distribution of the pressure in the SZ

$$F_l = \int_S p(r,\varphi,z)\cos(\tilde{\ }$$

$$\int_S$$

, (15)

where $p(r,\varphi,z)$ is the distribution of the pressure at the work contact area of the pin surface $S$; $\tilde{\ }$ is the current angle between the normal to the pin surface and the welding direction.
The tool torque is determined by the heat generation power in the SZ

$$M_P = \frac{1}{\omega_w}\int_{V_P} q_\Sigma \, dV_P, \tag{16}$$

where $q_\Sigma$ is the total heat generation rate in the SZ; $V_P$ is the volume of the SZ.

## MATERIAL PROPERTIES

All the temperature dependencies, needed for simulation, namely the heat conduction, enthalpy for the alloys AA5754 and AA6082 were received with the help of the program JMatPro® in the temperature range 20 $^0$C – solidus temperature for AA5754 (about 600 $^0$C) based on their chemical compound [22]; the reference yield strength for AA5754 is also taken from [22] fig. 5. The temperature and strain rate dependent dynamic viscosity and flow shear stress for AA5754 are derived from a series of special spot-FSW trials [16] (see below). As the metal of the stir zone in the model is considered as an incompressible viscous fluid (AA5754), its density is taken as temperature independent and constant at 20 $^0$C – 2.67 g/cm$^3$.

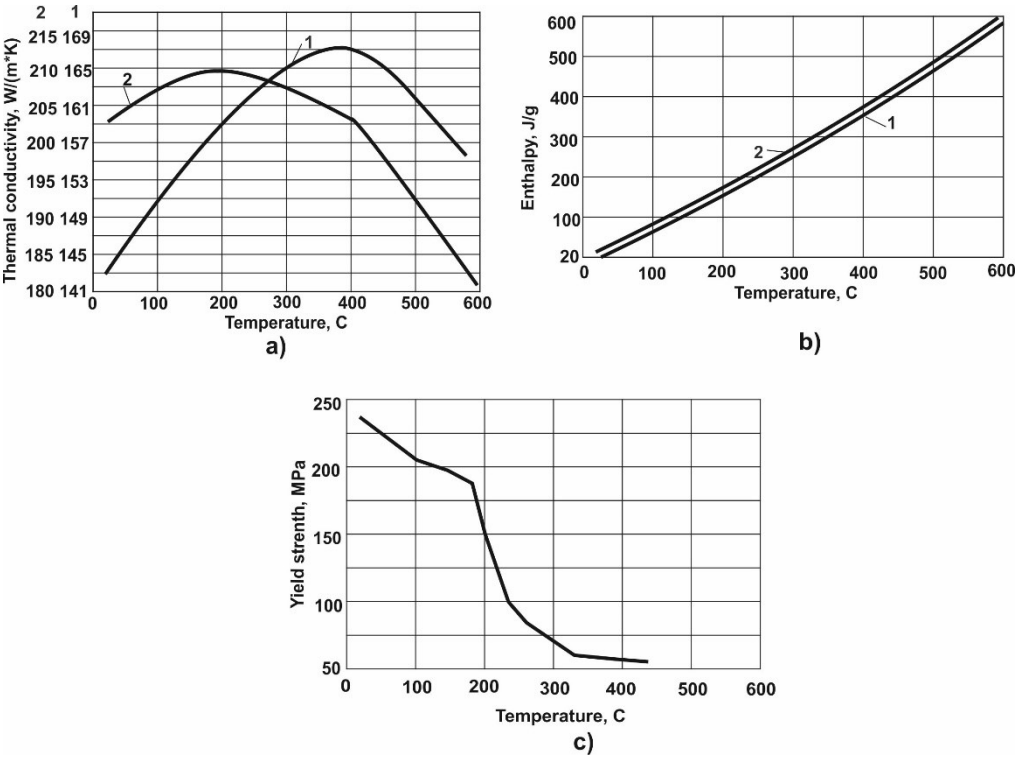


**Fig. 5** Thermophysical properties for AA5754 (1) and AA6082 (2) (a, b); the reference yield strength for AA5754 (c).

The dynamic viscosity (or the coefficient of the internal friction) is equivalent to the hardening rate at deformation

$$\eta(T, \dot{} \quad \tilde{} \quad \cdot \quad \frac{\prime}{\cdot}$$

(17)

where $k_\varepsilon$ is the empirical coefficient; $\tilde{\ }$ is the shear stress flow in dependence on the temperature $T$ and strain rate $\dot{\varepsilon}$; is the parameter accounting for hardening strain rate of the alloy at its deformation in the conditions of FSW.

The strain properties are described by the dependence of the flow shear yield strength on the temperature $T$ and the strain rate $\dot{\varepsilon}$

$$\tilde{\ } \quad \left(1 + k_1 \frac{\cdot}{\cdot}\right), \tag{18}$$

where $k_0$ is the coefficient takes into account the difference between $\tilde{\ }$ in the conditions of FSW and $\tau(T,0)$; $\tau(T,0)$ is the temperature dependence of the shear yield strength at $\dot{\varepsilon} = 0$; the coefficient $k_1$ accounts for the work hardening of the alloy.
The values of the coefficients for AA5754 $/s$, $k_1$=0.9, $k_\varepsilon = 0.35$ were calculated, using the basic experimental methodology for determining the mechanical characteristics adapted from [16]. The reference shear yield strength is defined by a theoretical relationship $\tau(T,0) = \frac{1}{\sqrt{3}}\sigma(T,0)$ [19].

## METHOD AND ALGORITHM OF NUMERICAL SOLUTION

We used the finite difference method for the numerical solution of the model equations. The program code was written in the object-oriented environment Embarcadero Delphi 2010. During the solution procedure, the methodology of successive iterations was applied until achievement of a quasi-stationary condition in the position of the SZ, as well as in the distributions of the flow velocities, heat generation, temperature and pressure. Table 1 represents the structure of the algorithm.

**Table 1** The algorithm of the numerical solution of the model equations

| |
|---|
| Input of the initial data: alloy, workpiece thickness, tool dimensions, angular velocity, welding speed, axial force |
| Reading thermophysical and reference mechanical properties from a database |
| Initial conditions on temperature, pressure, flow velocities and strain rate |
| Time-iterative loop $t=1..t_{max}$ |
| Calculation of the enthalpy, heat conduction and shear yield stress |
| Calculation of the heat generation power |
| Solution of the Navier-Stokes equations with boundary conditions. Consequent calculation of pressure, flow velocity and strain rate distributions |
| Solution of the energy equation and calculation of the temperature distribution |
| Variation procedure for specifying the boundaries of the SZ $P \cap W$ |
| $(t_{k+1}=t_k+1)$ until a quasi-stationary condition of the temperature and sizes of the SZ is reached |
| Output of the modelling results |

## RESULTS AND DISCUSSION

### SOME MODELLING RESULTS

The modelling results were obtained for a butt aluminium workpiece (AA5754, thickness 1.5+1.5 mm) with the tool depicted in fig. 4. The welding conditions were those as specified in table 2. The modelling results are presented in a form of weld macrosections, torque values as well as distributions and graphs:

- temperature distribution $T(r,\varphi,z)$ (fig. 6, trial N6 from table 2);
- relative pressure and strain rate $\left(p+p_N\right)/p$ , (fig. 7, 8, trial N6 from table 2);
- components of the flow velocity vector $v_r, v_\varphi, v_z$ (fig. 9, trial N6 from table 2);
- dependence of the tool torque and force components $F_l$ and $F_t$ on $\omega_w$ (fig. 10, a, b);
- dependence of the tool torque and force components $F_l$ and $F_t$ on $v_w$ (fig. 10, c, d).

**Table 2** Welding conditions for the modelling and experiment

| N | Welding conditions | Experimental weld macrosection (a)* | Modelled weld macrosection (b)* |
|---|---|---|---|
| 1,a,b | $v_w$ = 0.05 m/min<br>$\omega_w$ = 1000 r/min<br>$F$ = 14 kN | $S_{exp}$ = 5.6 mm$^2$<br>$M_{exp}$ = 7.50 N*m | $S_{mod}$ = 6.0 mm$^2$;<br>$M_{mod}$ = 8.5 N*m; |
| 2,a,b | $v_w$ = 0.08 m/min<br>$\omega_w$ = 1750 r/min<br>$F$ = 14 kN | $S_{exp}$ = 4.8 mm$^2$<br>$M_{exp}$ = 7.20 N*m | $S_{mod}$ = 5.2 mm$^2$;<br>$M_{mod}$ = 8.00 N*m; |
| 3,a,b | $v_w$ = 0.10 m/min<br>$\omega_w$ = 2000 r/min<br>$F$ = 14 kN | $S_{exp}$ = 4.6 mm$^2$<br>$M_{exp}$ = 6.99 N*m | $S_{mod}$ = 4.9 mm$^2$;<br>$M_{mod}$ = 7.49 N*m; |
| 4,a,b | $v_w$ = 0.15 m/min<br>$\omega_w$ = 2000 r/min<br>$F$ = 14 kN | $S_{exp}$ = 4.9 mm$^2$<br>$M_{exp}$ = 7.20 N*m | $S_{mod}$ = 4.7 mm$^2$;<br>$M_{mod}$ = 7.51 N*m; |
| 5,a,b | $v_w$ = 0.20 m/min<br>$\omega_w$ = 2750 r/min<br>$F$ = 12 kN | $S_{exp}$ = 4.5 mm$^2$<br>$M_{exp}$ = 6.48 N*m | $S_{mod}$ = 4.2 mm$^2$;<br>$M_{mod}$ = 6.80 N*m; |
| 6,a,b | $v_w$ = 0.25 m/min<br>$\omega_w$ = 3000 r/min<br>$F$ = 10 kN | $S_{exp}$ = 4.1 mm$^2$<br>$M_{exp}$ = 6.10 N*m | $S_{mod}$ = 4.0 mm$^2$;<br>$M_{mod}$ = 6.25 N*m; |

*$S_{exp}, M_{exp}$ – area of the SZ on the experimental weld macrosection and torque; $S_{mod}, M_{mod}$ – area of the SZ on the modelled weld macrosection and torque; Plunge depth = 1.1 mm. Butt joints (1.5 + 1.5 mm)

The modelling results show that the distributions of temperature (see fig. 6), relative pressure (see fig. 7), strain rate (see fig. 8) and viscous flow velocities (see fig. 9) have an asymmetric form relative to the tool longitudinal axis and welded joint surface. This asymmetrical form originates from the superposition of the translational and rotational welding velocities.

The gradients of the viscous flow govern the distribution of the strain rate and temperature. The maximum values of these distributions take place close to the workpiece surface in the contact with the tool and coincide in their shape, as the rate of the heat generation is proportional to the strain rate (see fig. 6, 8). The maximum of the relative pressure is, on contrary, displaced relative to the weld joint line against the tool rotation direction. It is explained by the fact that the metal in the zone of the lower temperatures possesses higher strength and therefore produces higher mechanical resistance (relative pressure) to the mass flow.

The motion of the tool surface, the pressure distribution and the form of the SZ defines the distribution of the metal viscous flow in the SZ.

The radial component of the viscous flow $v_r$ (see fig. 9 a) is mainly determined by the translational welding speed, i.e. by the flow of the viscous metal around the pin. Therefore, the metal in front of the pin moves back from the pin surface. Correspondingly, the metal behind the pin moves towards the pin rear surface.

The tangent component $v_\varphi$ (see fig. 9 b) arises from the tool rotational motion. Its asymmetrical distribution is explained by the different values of the pressure and distances form the pin surface to the boundary of the SZ. The tangent component $v_\varphi$ reaches its maximum values near the pin and shoulder surfaces in the direction of rotation.

Despite the use of the threadless pin, the axial component of the flow velocity $v_z$ arises in the SZ, which stems from the asymmetrical shape of the SZ and appearance of the axial pressure. The values $v_z$ are relatively small compared to the angular and radial ones. Moreover, the axial velocity rise with an increase in the $v_w$ and fall down with an increase in the $\omega_w$. The viscous metal moves down in front of the pin, reaching maximum values at the end of the pin. Correspondingly, behind the pin, the viscous metal flows upwards. The obtained results agree qualitatively with the literature data [19, 24].

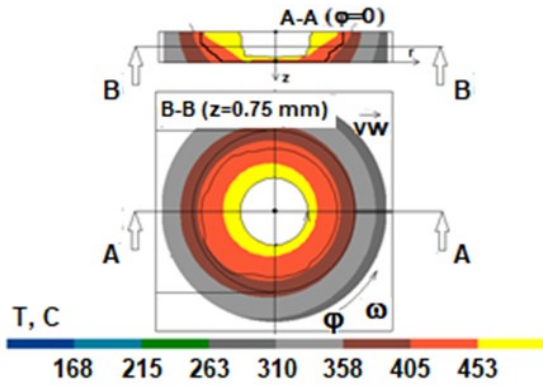


**Fig. 6** Temperature distribution.

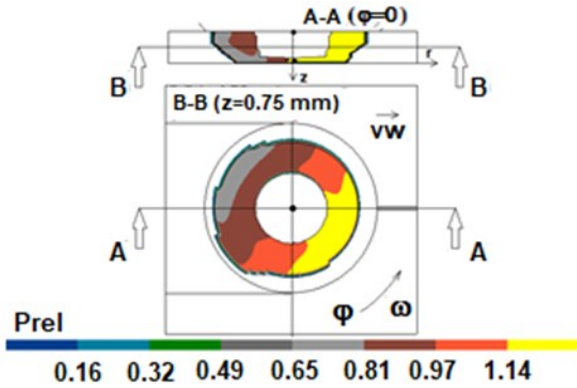


**Fig. 7** Distribution of the relative pressure in the stir zone.

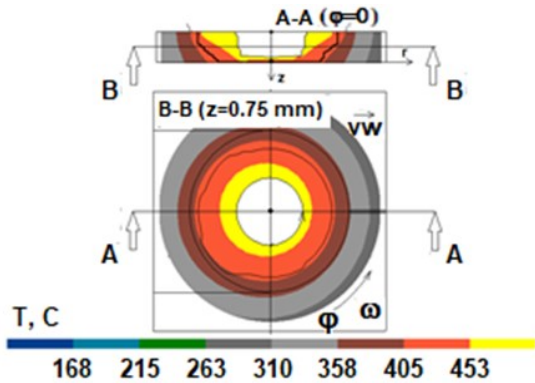


**Fig. 8** Distribution of the strain rate in the stir zone.

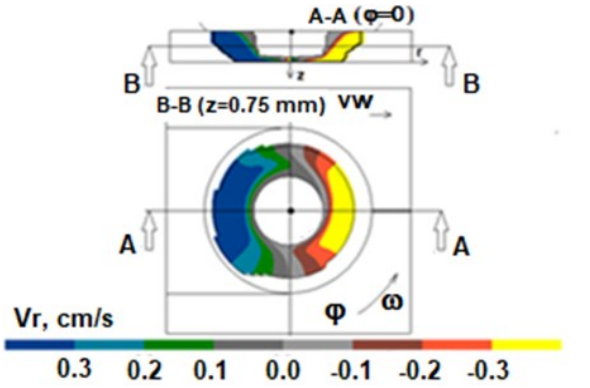


a)

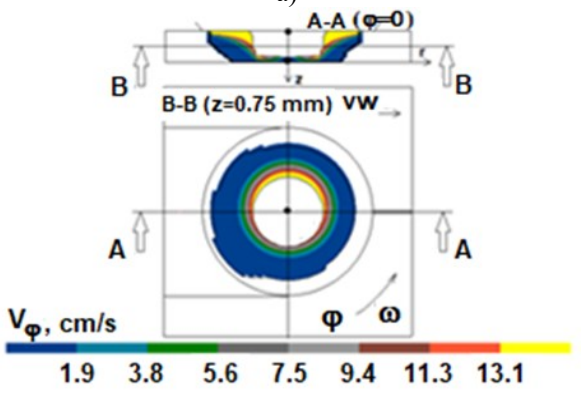


b)

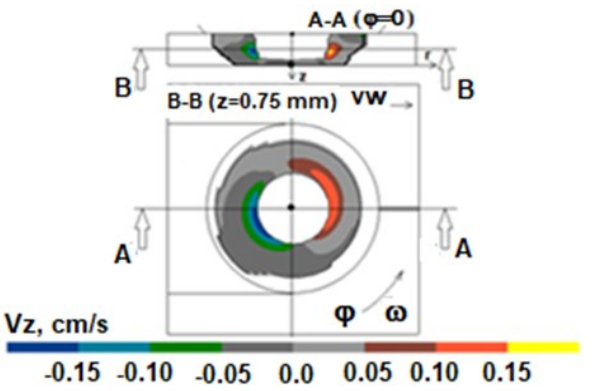


c)

**Fig. 9** Distributions of the components of the flow velocity vector: radial $v_r$ (a), tangent $v_\varphi$ (b), axial $v_z$ (c).

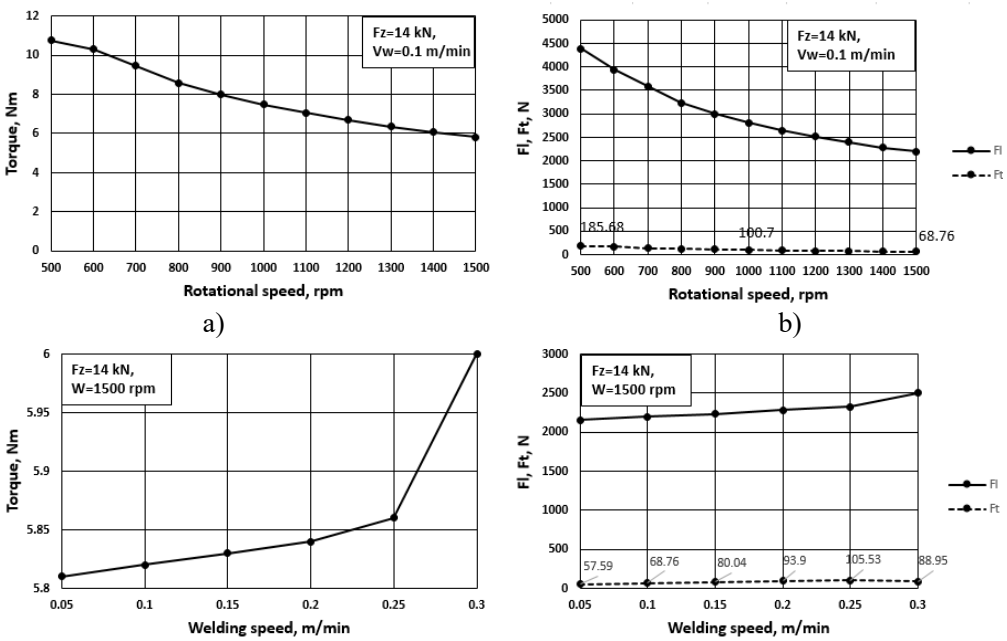


**Fig. 10** Graphs of the influence of the rotational (a, b) and welding speed (c, d) on the torque $M$ and force components $F_l$, $F_t$.

The model reproduces qualitatively correct the trend in the influence of the rotational and welding speed on the torque and tool force components (see fig. 10), which corresponds to the literature data ([25], for example). Particularly, an increase in the rotational speed causes an increase in the power of the heat generation. The temperature of the metal rises and its strength decreases. Therefore, the power for the rotation (torque $M$) and translation (forces $F_l$, $F_t$) of the tool becomes less. On the contrary, an increase in the welding (translational) speed causes an increase in the torque and the tool force components ($F_l$, $F_t$).

## COMPARISON WITH THE EXPERIMENTS

The experimental macrosections were also produced in order to compare the area of the SZ with the corresponding calculated values, fig. 11 (the welding conditions are those from table 2). A scatter plot depicting the experimental values versus the calculated ones, fig. 12-13, presents a comparison of the SZ shapes on the transversal weld macrosections as well as the corresponding torque values.

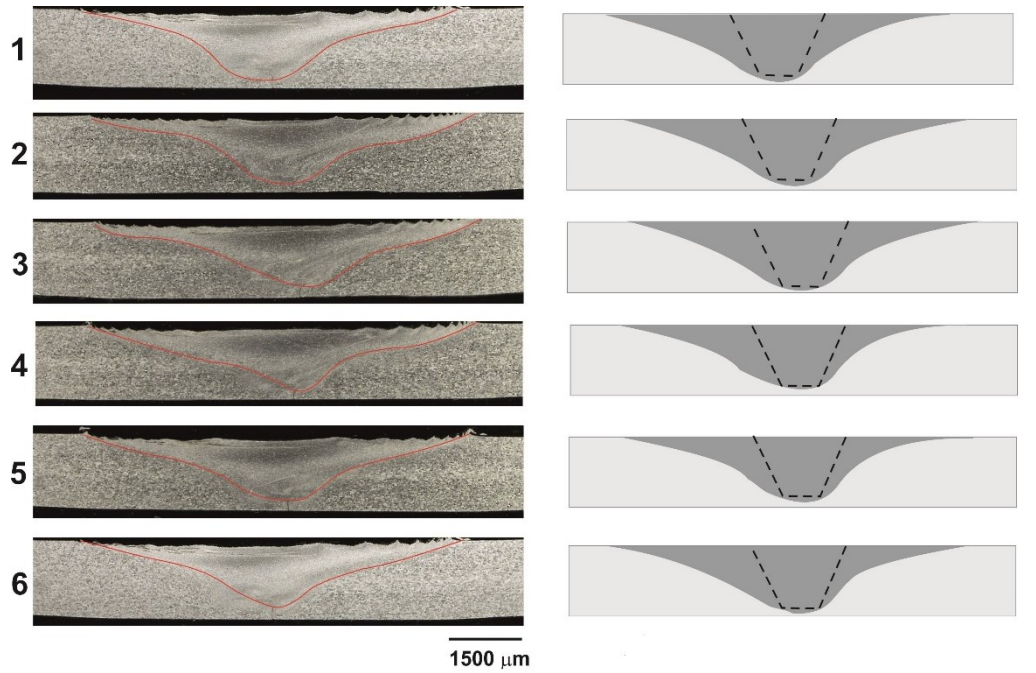


**Fig. 11** Comparison between the experimental (left part) and modelled (right part, outlined and scaled) weld macrosections.

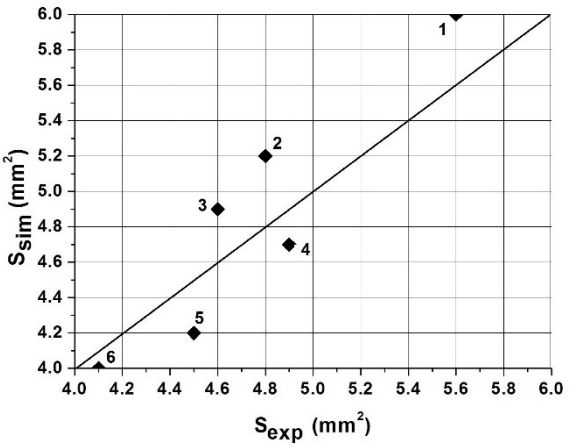


**Fig. 12** Scatter plot of the calculated values (vertical axis) of the stir zone area relative to the experimental data (horizontal axis).

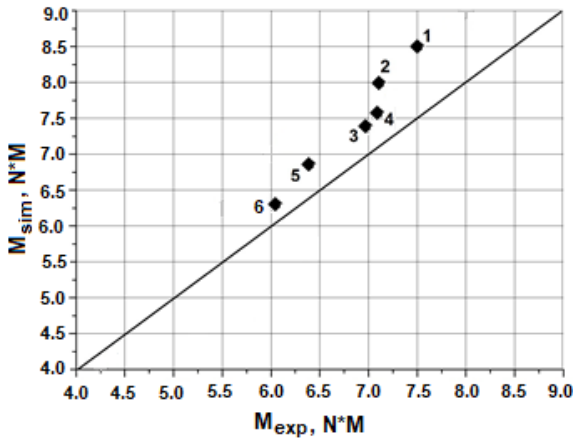


**Fig. 13** Scatter plot of the calculated values (vertical axis) of the torque relative to the experimental data (horizontal axis).

The comparison showed that the model satisfactorily reproduces the influence of the main welding conditions on the stir zone shape.

The location of the SZ boundary line is influenced by the distribution of the pressure in the SZ (axial from the tool and kinematic from the tool motion and rotation) as well as by the yield stress of the metal of the SZ. The latter is particularly temperature dependent. Therefore, the observed discordance could be explained by an inaccuracy in the values of the mechanical characteristics of the workpiece metal (AA5754), which requires the conduction of additional and modified mechanical tests [16] together with supplementary measurements of torque and thermo-cycles in a broader range of the process parameters.

## ACKNOWLEDGEMENTS

The authors would like to thank the German research society (DFG) for the support in conducting the work (Project RE 2755/50 “Investigation of the voids formation process in friction stir welding by numerical modeling and experiment on the basis of a Stress-condition hypothesis”).

## REFERENCES

[1] THOMAS W.M, NICHOLAS E.D, NEEDHAM J.C, MURCH M.G, TEMPLE-SMITH P, DAWES C.J.: ‚Friction stir butt welding’, *International Patent Application No. PCT/GB92/02203*, 1991.

[2] MORAITIS G. A., LABEAS G. N.: ‘Investigation of friction stir welding process with emphasis on calculation of heat generated due to material stirring’, *Science and Technology of Welding and Joining*, Vol. 15, pp. 177-184, 2010.

[3] GEMME F., VERREMAN Y., DUBOURG L., JAHAZI M.: ‘Numerical analysis of the dwell phase in friction stir welding and comparison with experimental data’, *Mater Sci Eng A*, 527:4152–60. DOI: 10.116/j.msea.2010.03.026.

[4] XIAOCONG H., FENGSHOU G., BALL A.: ‘A review of numerical analysis of friction stir welding’, *Progress in Materials Science*, Vol. 65, pp. 1-66, 2014.

[5] RUSSELL, M.J., SHERCLIFF H.R.: 'Analytical Modeling of Friction Stir Welding', *Prec., INALCO '98: 7th Intl. Conf.: Joints in Aluminum*, Cambridge, UK, 16 April 1998, Vol.2, pp. 185-195.
[6] GOULD J.E., Z. FENG.: 'Heat flow model for friction stir welding of aluminum alloys'. J. Mater. Process. Manuf. Sci. 1998, 7, pp. 185-194.
[7] SCHMIDT H., HATTEL J.: 'An analytical model for the heat generation in friction stir welding', *Modelling Simul. Mater. Sci. Eng*., 12 (2004), pp. 143-157.
[8] FRIGAARD Ø., GRONG Ø., MIDLING O.T.: 'A Process Model for Friction Stir Welding of Age Hardening Aluminium Alloys', *Metall. Mater. Trans A*. May 2001; 32 (5), pp. 1189-1200.
[9] CHAO Y.J., QI X., TANG W.: 'Heat transfer in friction stir welding: experimental and numerical studies', *ASME J. Manuf. Sci. Eng*. 125 (2003), pp.138-145.
[10] SEIDEL T.U., REYNOLDS A.P.: 'Two-dimensional friction stir welding process model based on fluid mechanics', *Sci. Technol. Weld. Join*., 2003, 8(3), pp. 175-183.
[11] COLEGROVE P.A., SHERCLIFF H.R.: 'Development of Trivex friction stir welding tool. Part 2 – three-dimensional flow modelling', *Science and Technology of Welding and Joining*, 2004, Vol. 9, No. 4, pp. 352-361.
[12] COLEGROVE P.A., SHERCLIFF H.R.: '3-Dimensional CFD modelling of flow round a threaded friction stir welding tool profile', *J. Mater. Process. Technol*., 2005, 169, (2), pp. 320-327.
[13] TUTUNCHILAR S., HAGHPANAHI M., BESHARATI GIVI M.K., et al.: 'Simulation of material flow in friction stir processing of a cast Al–Si alloy', *Mater. Des.* 2012; 40, pp. 415-426.
[14] TARTAKOVSKIY A., GRANT G., SUN X., KHALEEL M.: 'Modeling of friction stir welding (FSW) process with smooth particle hydrodynamics (SPH)'. *In: SAE 2006 World Congress, Detroit, USA.*
[15] PAN W.X., LI D.S., TARTAKOVSKY A.M., AHZI S., KHRAISHEH M., KHALEEL M.: 'A new smoothed particle hydrodynamics non-Newtonian model for friction stir welding: process modeling and simulation of microstructure evolution in a magnesium alloy', *Int. J. Plast*., 2013, 48, pp. 189-204.
[16] HENNEBÖHLE U.: 'Verifizierung und Bewertung eines thermischen Simulationsmodells des Rührreibschweißprozesses', *Aachen: Shaker*, 2008.
[17] EROFEEV V., MASLENNIKOV A.: 'Fiziko-matematicheskaya model svarki treniem s peremeshivaniem [Physical and mathematical model of the friction stir welding process]', *Izvestiya Tulskogo gosudarstvennogo universiteta (Technicheskie nauki)*, Vol. 10, pp. 64-73, 2013 [in Russian].
[18] MISHRA R.S., DE P.S., KUMAR N.: 'Friction stir welding and processing', *Science and engineering*, *Springer*, Vol. 16-17, 2014.
[19] NANDAN R., ROY G.G., DEBROY T.: 'Numerical simulation of three-dimensional heat transfer and plastic flow during friction stir welding', *Metallurgical and Materials transactions A*, Vol. 37A, pp. 1247-1259, 2006.
[20] SCHMIDT H., HATTEL J., WERT J: 'An analytical model for the heat generation in friction stir welding', *Model. Simul. Mater. Sci. Eng.*, Vol. 12, pp. 143-157, 2004.
[21] VIJAY SHIVAJI GADAKH, KUMAR ADEPU: 'Heat generation model for taper cylindrical pin profile
in FSW', *J. Mater. Res. Technol.*, 2(4), pp. 370-375, 2013.
[22] DEMIRAY Y., KAVAKLIOGLU Z.B., Y. YUCEL: 'A study on thermo-mechanical behaviour of AA5754 alloy (tread and plain sheet) produced by twin-roll casting', *Acta Physica Polonica A*, Vol. 127, pp. 1097-1099, 2015.
[23] BOOSTER R.E.: 'Handbook of lubrication', *CRC Press LLC*, pp. 46-47, 1983.
[24] GRUJICIC M., ARAKERE G, YALAVARTHY H.V. et al.: 'Modeling of AA5083 material-microstructure evolution during butt friction-stir welding', *Journal of Materials Engineering and Performance*, Vol. 19(5), pp. 672-684, 2010.

[25] SHAHI P., BARMOUZ M.: 'Force and torque in friction stir welding', *Advances in Friction Stir Welding and Processing. Elsevier Limited*, DOI: 10.1533/9780857094551.459, pp. 459-498, 2014.